Density functional theory studies on covalent functionalization of single-walled carbon nanotubes with benzenesulfonic acid

ARTICLE *in* VIBRATIONAL SPECTROSCOPY · MARCH 2013

Impact Factor: 2 · DOI: 10.1016/j.vibspec.2012.12.003

1 AUTHOR:

Metin Aydin
Ondokuz Mayıs Üniversitesi
32 PUBLICATIONS **171** CITATIONS

SEE PROFILE

Vibrational Spectroscopy 65 (2013) 84–93

Contents lists available at SciVerse ScienceDirect

Vibrational Spectroscopy

journal homepage: www.elsevier.com/locate/vibspec

Density functional theory studies on covalent functionalization of single-walled carbon nanotubes with benzenesulfonic acid

Metin Aydin*

Department of Chemistry, Faculty of Art and Sciences, Ondokuz Mayıs University, Kurupelit, Samsun 55139, Turkey

ARTICLE INFO

Article history:
Received 9 July 2012
Received in revised form 6 December 2012
Accepted 7 December 2012
Available online 20 December 2012

Keywords:
SWCNT
DFT calculation
Nanotube
Raman
IR
Charge transfer

ABSTRACT

The calculated Raman spectra of the covalently functionalized zigzag single-walled carbon nanotubes, f-(n,0)-SWCNTs (n = 6–10), with benzenesulfonic acid showed that the radial breathing modes (RBMs) frequencies (ω_{RBM}) of the sidewall functionalized tubes are red shifted in comparison with the frequencies of their non-functionalized counterparts, (n,0)-SWCNTs. It is also observed that this ω_{RBM} red-shift is tube-diameter (d_t) dependent, where almost no redshifts are observed for the (10,0)-SWCNT. Moreover, many new Raman bands, which results from the functional group, appear in the low energy region, ranging from 100 to 600 cm^{-1}. In the high frequency region, resulting from the functional group, the Raman spectra of the f-(n,0)-SWCNTs exhibited a few new peaks above the tangential bands of the SWCNTs (ranging from 1580 to 1650 cm^{-1}), which entirely belongs to the C—C stretching, including bending deformation of the CCC bonds, and rock of CH in phenyl group of the benzenesulfonic acid as well as many new Raman peaks dispersed through spectrum. The calculated IR spectra also exhibited many new peaks through spectra of the f-(n,0)-SWCNT when comparing these with corresponding IR spectrum of the isolated nanotube. Furthermore, the calculated vertical singlet-singlet electronic transitions of the f-(n,0)-SWCNTs significantly altered in the optical structure of the nanotube and exhibited charge transfer states for both the functionalized (8,0)- and (12,0)-SWCNTs. The small distances among the calculated dipole-allowed and forbidden electronic energy levels also suggested an internal crossing (IC) processes.

1. Introduction

Carbon nanotubes (CNTs) were discovered in 1991 [1], their unique physical, chemical, and electronic properties have led to a variety of technological application in functional nanodevices, especially as transistors and sensors [2–7], in heat conduction systems [8,9], in specialty electronics [10,11], molecular memories [12], optics [13–15], electrically excited single-molecule light sources [16–19], biomolecules such as DNAs (deoxyribonucleic acid) and proteins may nonspecifically bind to the surfaces of SWNTs due to hydrophobic interactions and p–p stacking interactions [20–22], high-performance adsorbent electrode material for energy-storage device [23], and protein functionalization [24,25].

As it is well known, carbon nanotubes can be obtained as being formed by rolling up a defined projected area from the hexagonal lattice of a graphene sheet in a seamless fashion such that all carbon–carbon (C—C) valences are satisfied, and the direction in which the roll up is performed gives rise the circumference of the tube. The projected area is in fact a homomorphic representation of a particular carbon nanotube [26,27]. The roll-up vector is also called the chiral vector, and is defined as $n\vec{a}_1 + n\vec{a}_2$, where $n\vec{a}_1$ and $n\vec{a}_2$ are the unit vectors of the hexagonal lattice of the graphene sheet, and n and m are the so-called chiral indices. An infinite number of nanotube geometries are possible, being a specific nanotube fully characterized by its chiral indices (n,m), which, in turn, define the nanotube chiral angle θ and tube diameter (d_t); the latter is dependent on the C—C bond length of the graphene hexagonal lattice. For $n = m$, the nanotube is known as “armchair”, while for $n \neq 0$ and $m = 0$, the nanotube is called “zigzag”; while for $n \neq 0$ and $m \neq 0$ the nanotube is known as “chiral.” The diameters of the nanotube normally present values that range from 0.4 nm to above 3 nm for SWCNTs and from ~1.4 nm to at least 100 nm for MWCNTs, while nanotubes are usually several microns in length. It is worth noting that single-walled and multi-walled carbon nanotubes generally have properties that are significantly different, while double-walled carbon nanotubes (DWCNTs) can be viewed as representing the key structure that defines the transition between SWCNTs and MWCNTs.

Carbon nanotubes (CNTs) can be metallic or semiconducting depending on their structure. This metallicity is due to the symmetry and the unique electronic structure of graphene. If the chiral indices are equal, $n = m$, the nanotube is metallic; if $n - m$ is a

* Tel.: +90 312 3621919x5522; fax: +90 3624576081.
E-mail address: aydn123@netscape.net

0924-2031/$ – see front matter © 2012 Elsevier B.V. All rights reserved.
http://dx.doi.org/10.1016/j.vibspec.2012.12.003

multiple of 3, then the nanotube is semiconducting; otherwise, the nanotube is a semiconductor [28]. Interestingly, some nanotubes have conductivities higher than that of copper, while others behave more like silicon.

As is well known, the optical properties of nanotubes can be efficiently studied by means of the absorption, photoluminescence, and Raman spectroscopy [29,30]. Such optical measurements permit a reliable characterization of the quality of nanotube, such as chirality, size, and structural defects. In the case of Raman measurements, even though a large number of phonon modes of carbon nanotubes is expected, most of them are Raman inactive due to the selection rules that emanate from the high symmetry properties of the nanotubes. The Raman spectrum of a CNT exhibits a few characteristic modes that can be used to determine the size of nanotubes and to classify their metallicity, e.g., if the CNT is semiconducting or metallic. For example, in the low frequency region of the CNT spectra, one type of characteristic vibration is called the radial breathing mode (RBM); in the RBM, the movement of the carbon atoms is in the radial direction with the same phase, and corresponds to vibration of the entire tube, whose frequency is strongly diameter dependent. The RBM gives precise information about the nanotube diameter and is typically found between 100 cm^{-1} and 500 cm^{-1} [26,27]. Additionally, in the high energy range from (1000 to 2000 cm^{-1}), there are two important characteristic Raman bands: the defect induced disordered band (D-band) that appears between 1300 and 1400 cm^{-1}, and tangential modes (G-band) that lie in the range from ~1560 to ~1600 cm^{-1}. The D-band is present in all graphite-like carbons and originates from structural defects. Therefore, the intensity ratio of the *G*/*D* modes is conventionally used to quantify the structural quality of carbon nanotubes. The G-band corresponds to planar vibrations of carbon atoms and is present in most graphite-like materials (at around 1580 cm^{-1}). This tangential mode (G-band) in SWCNT is split into several peaks. The splitting pattern and intensity depend on the tube structure and excitation energy; they can be used, though with much lower accuracy compared to RBM mode, to estimate the tube diameter and whether the tube is metallic or semiconducting [26,27,31].

Chemical functionalization by bond formation, coating of the nanotubes with organic/inorganic molecules or by encapsulating a variety of semiconductor particles, including CdSe and CdTe, may lead to efficient energy transfer between the molecules and nanotube, as well as lead to significant enhancement in the optical properties of the composite system [32–35]. As an example, it has been reported that when a squarylium dye is encapsulated into a carbon nanotube, an increased chemical and thermal stability of squarylium molecules occur, since encapsulation of a dye quenches the strong dye luminescence, which allows measurement and analysis of the dye's Raman spectra [36]. Also, Alvarez et al. [30] have reported that while infrared spectroscopy (IR) might provide evidence of a significant positive charge transfer for an inserted oligothiophene, Raman spectra evidence different behaviors depending on the excitation energy and on the relationship to the oligomer's (specifically, quaterthiophene) optical absorption energy. For example, at high excitation wavelength (647.1, 752, and 1064 nm; far from the oligomer's resonance at ~400 nm), radial breathing modes exhibit a significant blue-shift as a result of the encapsulation effect, while at low excitation wavelength (514.5, 488, and 458 nm), close to resonance with the oligomer absorption, both the CNTs G-band and the low-frequency modes (below 300 cm^{-1}) vanish, suggesting a significant charge transfer between the oligomer and the nanotube. It is worth noting that positive charge transfer process has generally been considered to occur by direct transfer of an electron from one system which becomes a cation to other system (neutral/cation) which becomes anion/neutral.

Moreover, CNTs are also widely used in the research medical area. The CNTs are observed to enhance the drug delivery in bio-systems as they are applied in, for health monitoring devices. They are also used as biosensing platforms for the treatment of various diseases and in chemical sensor devices, etc. [37–40]. Functionalized-SWCNTs (f-SWCNTs) have been known to increase solubility and to permit efficient tumor targeting/drug delivery, the functionalization also prevents SWCNTs from being cytotoxic and CNT possibly alter the functioning of immune cells. Moreover, CNTs have enhanced solubility when functionalized with lipids which make the CNT motion through the human body easier, reducing the risk of blockage of vital body organ pathways. Also, CNTs exhibit strong optical absorbance in certain spectral windows, such as the NIR (near-infrared); when functionalized within tumor cell with specific binding entities. This strong absorption of the nanotubes have allowed the selective destruction of sick cells (e.g., cancerigenous cells) with NIR in drug delivery applications [41].

For functionalized single-walled carbon nanotubes (f-SWCNTs), we find that there should be a charge transfer process from the nanotube to an attached molecule, which is optical active. Generally, upon irradiation a system can undergo internal conversion (IC) and intersystem crossing (ISC) processes [48], in addition to photochemical and other photophysical processes. Transient intermediates are likely to be formed in the IC and ISC radiationless processes, herein referred to as "dark processes," which are not detected using conventional light absorption or emission spectroscopic methods. For a typical molecule the emission of a photon from an electronically excited state to the ground state results in a broad fluorescence signal in the region of 300–1500 nm. Photophysical processes for an isolated molecule occur as a result of transitions between the different internal energy states, which comprise the electronic states. A molecular system in the gas-phase or in the solution phase at room temperature is mostly expected to be in its ground state (S_0). The excitation of a molecular system from its ground state to an excited vibroelectronic state by absorption of a photon (occurring within ca. 10^{-15} s) is much faster than a emission of the photon from its excited electronic state (S_k, $k > 1$) to its ground state (occurring in ca. 10^{-8} s). Most excited molecular systems may not directly return to their ground state by emission of a photon ($S_{k>0} \rightarrow S_0$ transition). Some systems may return to their ground states (S_0) by internal conversion (CI). For instance, when the molecule is excited into a higher vibroelectronic state (S_k, $k > 1$), it may undergo relaxation to the S_1 state (in 10^{-12} s) via vibrational coupling along these (S_k, $k > 1$)states before undergoing additional vibrational relaxation and returning to the lowest singlet electronic energy level (S_1), a process named as internal conversion (IC). Subsequently, the transition from S_1 to S_0 occurs by an emission of a photon (fluorescence). An alternative pathway for a molecule in the lowest excited energy S_1 state involves intersystem crossing (at rates that can compete with fluorescence) by the molecule into a triplet state T_1. From T_1, the molecule can undergo radiative de-excitation via a much slower process, which is known as phosphorescence ($T_1 \rightarrow S_0$ transition), such as illustrated by the Perrin–Jablonski diagram.

It is important to note that fluorescence resonance energy transfer (FRET) can be used to investigate intra- and/or intersystem energy transfer dynamics that might occur as transitions from single-walled carbon nanotubes (SWCNTs) to multi-walled carbon nanotubes (MWCNTs), as well as from the functionalized nanotubes (f-NTs). Such dark intermediates are expected to play crucial roles in IC and ISC processes and thus are fundamental to understanding photochemistry mechanism of the functionalized-nanotubes and multi-walled nanotubes.

Quantum mechanical calculations have been used to aid in the assignment of the vibrational bands of the experimentally measured Raman and IR spectra for functionalized and isolated

nanotubes in addition to their optical properties. In this study, we provide theoretical results on functionalized single-walled carbon nanotubes (f-SWCNTs) using density functional theory (DFT). Moreover, this report complements the quantum chemical computational approach that we have used earlier [26,27]. The results of our calculations not only indicate the shift in the spectral peak positions (frequencies) of the RBM and G-modes in Raman spectra of f-SWCNTs relative to their corresponding isolated SWCNTs, but also indicate a charge transfer mechanism, where the charge transfer is happening from the SWCNT to the functional group when f-SWCNT are excited to charge transfer state as discussed below.

2. Results and discussion

2.1. Computational methods

In order to obtain the lowest energy level (true ground state), the ground state geometries of the single-walled carbon nanotubes (SWCNTs) and the functionalized-SWCNTs (f-SWCNTs) were optimized without symmetry restriction on the initial structures. Both structure optimization and vibrational analysis calculations were implemented using density functional theory (DFT) with functionals, specifically, B3LYP (Becke Three Parameter Hybrid Functionals), in which the exchange functional is the Becke's three parameter type, including gradient correction, and the correlation correction involves the gradient-corrected functional of Lee, Yang and Parr [42]. The basis set used is split valence type 6-31G, as contained in the Gaussian 03 software package [43]. The results of the calculations did not produce any imaginary frequencies. The vibrational mode descriptions were made on the basis of the calculated nuclear displacements using visual inspection of the animated normal modes (using the GaussView03 software) [44], to assess which bond and angle motions dominate the mode dynamics for each nanotube. The DFT method was chosen because it is computationally less demanding than other approaches as regards inclusion of electron correlation. Moreover, in addition to its excellent accuracy and favorable computation time, the B3LYP calculation of Raman frequencies has shown its efficacy in numerous earlier studies performed in this laboratory and by other researchers, often proving the most reliable and preferable method for many molecular species of intermediate size, including anions and cations [26,27,45–50]. In our calculations, hydrogen atoms have been placed at the end points of the unit cells. Furthermore, the time-dependent-DFT in the TD-B3LYP level was applied to calculate the vertical electronic transitions for the SWCNTs and functionalized (n,0)-SWCNTs. For geometry optimization and calculations of electronic transitions, the 6-31G* basis set was used for sulfur atom (S) and the 6-31G basis set was used for the other atoms involved in the covalently functionalized nanotubes.

3. Results of calculations

3.1. Zigzag-SWCNT covalently functionalized with benzenesulfonic acid

In this section, we calculate, for covalently functionalized zigzag single-walled carbon nanotubes (f-(n,0)-SWCNTs), their energy associated to the binding curvatures, IR and Raman spectra, and vertical electronic transitions. The latter one is important to understand the optical mechanism for the charge transfer between functional group(s) and (n,0)-SWCNTs as well as internal conversion (IC) and intersystem crossing (ISC), as well as photochemical process that may occur.

The structure of the functionalized zigzag single-walled carbon nanotubes, f-(n,0)-SWCNTs, constructed with functional group(s) covalently bound to the (n,0)-SWCNTs, whose length is equal to two unit cell length, have been investigated. The energetically most stable geometry has been obtained by means of their full optimization, without any symmetry restriction. The optimized structure indicated that the cylindrical shape of the nanotube is altered to an elliptical form when two molecules are covalently attached on the sidewalls of the (n,0)-SWCNT as seen in Fig. 5; but the structure remains almost cylindrical with C_4 symmetry, when four functional groups are chemically bound. Energetically more stable covalently functionalized (n,0)-SWCNT (f-(n,0)-SWCNTs; n = 6–12) was predicted from the energy difference (ΔE[f-(n,0)-SWCNTs]) between the total energy of the f-(n,0)-SWCNTs per the number of hexagons in the tube (E[f-(n,0)-SWCNT)/2n]) with reference to the total energy of their corresponding isolated (n,0)-SWCNTs per the number of hexagons in the tube, (E[(n,0)-SWCNT)/2n]) and the total energy of the functional groups (E(f)/2n) by using the following equation:

$$\Delta E[\text{f-}(n,0)\text{-SWCNTs : in eV}] = \frac{E[\text{f-}(n,0)\text{-SWCNT}]}{2n} - \frac{E[\text{f}] + E[(n,0)\text{-SWCNTs}]}{2n}$$

where the letters n and 2n stand for the chiral index of the zigzag-SWCNTs and the number of hexagon in the nanotube, respectively. The letter f stands for the benzenesulfonic acid (-ph-SO_3H; $-C_6H_4SO_3H$) was used as the functional group covalently bound to the sidewall of the (n,0)-SWCNTs. The plot of the calculated binding energy of the functional group, per the number of hexagon in the tube, is given in Fig. 1. As seen in Fig. 1, the binding energies of the functional groups for the metallic and semiconducting f-SWCNTs are well separated from each other. Based on the predicted the binding energies (E[f-(n,0)-SWCNTs]), the results suggested that the covalent functionalization of the (0,n)-SWCNTs with small diameters, is energetically more stable than that with large diameters for the metallic nanotubes. This finding is not so surprising since the disruption of π-electrons and the formation of sp^3-hybridized carbon on the nanotube wall, which is the character of the covalent functionalization, increases with decreasing

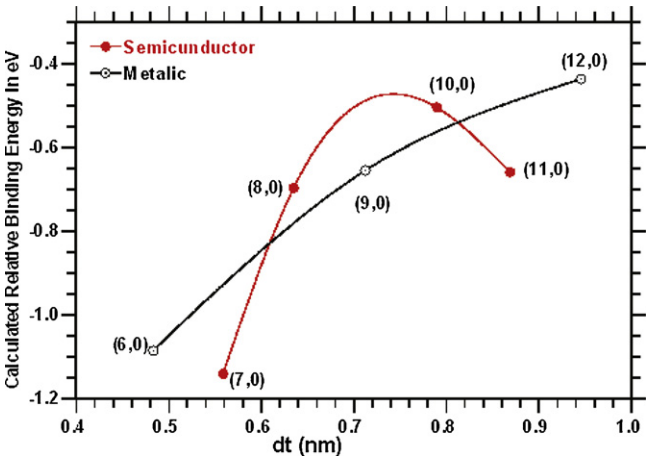

Fig. 1. Calculated binding energies of the (n,0)-SWCNTs covalently functionalizes with the benzenesulfonic acid ((n,0)-SWCNTs-ph-SO_3H, n = 6–12). Energetically more stable covalently functionalized (n,0)-SWCNT (f-(n,0)-SWCNTs; n = 6–12) was predicted by using the equation: E[f-(n, 0)-SWCNTs : in eV] = E[f-(n, 0)-SWCNT]/2n − E[f] + E[(n, 0)-SWCNTs]/2n. Where ΔE[f-(n,0)-SWCNTs] is the energy difference between the total energy of the f-(n,0)-SWCNTs per the number of hexagons in the tube (E[f-(n,0)-SWCNT)/2n]) with reference to the total energy of their corresponding isolated (n,0)-SWCNTs per the number of hexagons in the tube (E[(n,0)-SWCNT)/2n]) and the total energy of the functional groups (E(f)/2n). The letters n and 2n stand for the chiral index of the zigzag-SWCNTs and the number of hexagon in the nanotube, respectively. See Section 3.1 for more detail.

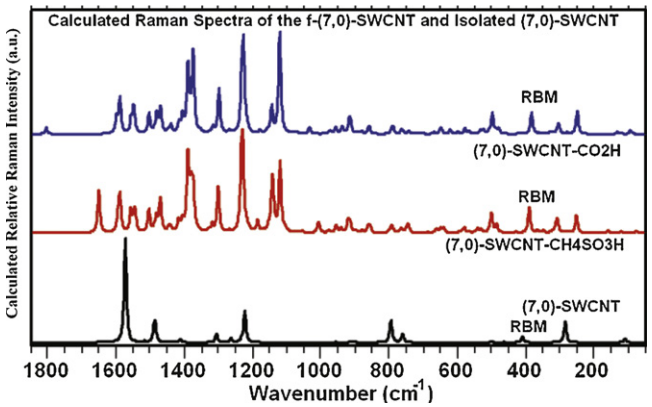

Fig. 2. Calculated Raman spectra of the (7,0)-SWCNT-ph-SO_3H, (7,0)-SWCNT-CO_2H, and isolated (7,0)-SWCNT with length equivalent to two unit.

tube's diameter. However, for semiconducting nanotubes, (7,0)-, (8,0), and (10,0)-SWCNT, the sidewall functionalization of the (*n*,0)-SWCNT with small diameter is energetically more stable than the functionalization of the (0,*n*)-SWCNT with large diameter, except for the f-(11,0)-SWCNT as seen in Fig. 1. In order to make a correct overall assessment, we need to more data, at least for semiconducting zigzag nanotubes.

3.2. Raman spectra of functionalized zigzag-SWCNTs

We calculated nonresonance Raman spectra of covalent sidewall functionalization of the (*n*,0)-SWCNTs with benzenesulfonic acid ((*n*,0)-SWCNT-ph-SO_3H) and the isolated (*n*,0)-SWCNTs (where $n = 6–10$), in addition to the Raman spectrum of sidewall functionalized (7,0)-SWCNT with the carboxylic acid ((7,0)-SWCNT-CO_2H) was calculated for comparison. As seen in Fig. S1 in supplementary information (SI), because of the similarity of the Raman spectra of the f-(*n*,0)-SWCNTs, here we discuss only the Raman spectra of the (7,0)- SWCNT-ph-SO_3H and (7,0)-SWCNT-CO_2H with reference to the spectrum of the isolated (7,0)-SWCNT. AS seen in Fig. 2, the Raman spectra of both (*n*,0)-SWCNT-ph-SO_3H) and (7,0)-SWCNT-CO_2H) exhibited many new features with reference to the spectrum of the isolated (7,0)-SWCNT in addition to shift in the peak positions along their Raman spectra. The results of the calculations are summarized below.

(a) The predicted common peaks in the spectra of the functionalized and isolated (7,0)-SWCNT: (1) two weak peaks at 109 and 111 cm^{-1} result from the elliptical deformation of the carbon nanotube are respectively shifted to 75 and 121 cm^{-1} in the Raman spectrum of the (7,0)-SWCNT-ph-SO_3H and to 95 and 134 cm^{-1} in the spectrum of the (7,0)-SWCNT-CO_2H, and no change in their relative intensities; (2) a medium intense peak at 284 cm^{-1} (as a result of diagonal expansion of the tube) is split into two well-separated peaks, which are shown at ~250 and 306 cm^{-1} in the spectrum of each (7,0)-SWCNT-ph-SO_3H and (7,0)-SWCNT-CO_2H, and no significant change in the intensity; (3) a medium intense Raman peak at 410 cm^{-1} in the isolated (7,0)-SWCNT, which is the characteristic mode of SWNTs is called as the radial breathing mode (RBM) that it is a commonly used technique to evaluate the diameter of carbon nanotubes, is shifted not only to 390 and 385 cm^{-1} in the spectra of the (7,0)-SWCNT-ph-SO_3H and (7,0)-SWCNT-CO_2H, respectively, but also, its relative intensity is enhanced in both spectra; (4) a very weak peak (almost vanish) at 500 cm^{-1} in the spectrum of the isolated tube is as a result of the bending deformations of CCC bond in the tube, which is predicted at 493 and 501 cm^{-1} in the Raman spectra of the (7,0)-SWCNT-ph-SO_3H and (7,0)-SWCNT-CO_2H, respectively, and its intensity is significantly enhanced in both spectra; (5) a relatively weak peak at 793 cm^{-1}, which is as a result of the out-of-surface bending deformation of the CCC bond in the tube, is shown at the same position in both spectra, but its relative intensity decreases; (6) a medium intense peak at 1223 cm^{-1} is caused by rocking of the Hs (hydrogen atoms) on the open-end point of the tube, which appears at 1230 cm^{-1} in both spectra (of (7,0)-SWCNT-ph-SO_3H and (7,0)-SWCNT-CO_2H); additionally, a significant enhancement in its relative intensity takes place; (7) a weak peak at 1305 cm^{-1} results from the CC bond stretching and bending deformation of the CCC bonds in the tube, which corresponds to a significantly enhanced peak at 1300 cm^{-1} in both spectra; (8) a very weak peak at 1411 cm^{-1}, as a result of the CC stretching and asymmetric stretching of the CCC bonds in the tube, is not only red shifted to 1389 (strong) and 1391 (strong) cm^{-1} in the spectra of the (7,0)-SWCNT-ph-SO_3H and (7,0)-SWCNT-CO_2H, respectively, but also, its relative intensity dramatically increases in both spectra; (9) a relatively weak peak at 1485 cm^{-1} is caused by CC stretching along tube axis, which is shown at 1482 cm^{-1} in both spectra and no change in its relative intensity; (10) the most strongest Raman peak (which is known as tangential or G mode) at 1574 cm^{-1} in the isolated (7,0)-SWCNT, resulting from CC stretching and bending deformation of the CCC bonds in the tube, is not only blue shifted to 1590 and 1595 cm^{-1} in the Raman spectra of the (7,0)-SWCNT-ph-SO_3H and (7,0)-SWCNT-CO_2H, respectively, but also, its relative intensity significantly decreased. The G-mode is one of the important vibrational modes in the Raman spectrum of the carbon nanotube for the reason that it is a commonly used technique to classify the metallicity of the carbon nanotubes.

(b) Calculated new Raman features in the spectrum of the (7,0)-SWCNT-ph-SO_3H: (1) two relatively strong peaks at 1119 and 1143 cm^{-1} are as a result of the symmetric stretching vibration of the CCC bonds (where – ph-SO_3H unit is covalently attached on the sidewall of the tube), including bending deformation of the CCC bonds in the tube and inplane rocking of Hs on the benzene ring; (2) a medium intense peak 1139 cm^{-1} is due to asymmetric stretching of C—S=O, and rocking of OH bond in the —SO_3H group, including structural deformation of the tube; (3) the relatively strong peak at 1373 cm^{-1} results from asymmetric stretching vibration of O=S=O and rocking of OH, including relatively weak asymmetric stretching of CCC bonds in the benzene ring; (4) a medium peak at 1502 cm^{-1} is caused by structural deformation of the tube; (5) a medium peak at 1543 cm^{-1} is due to symmetric stretching of the CCC bonds in the benzene ring and rocking of the Hs on the benzene ring, including the CC stretching and asymmetric stretching vibration of the CCC bonds in the tube; (6) the peak at 1547 cm^{-1} is caused by the symmetric stretching of CCC bonds in the benzene ring and rocking of CHs on the ring; (7) a medium peak at 1557 cm^{-1} is due to the stretching vibrations of the CC bonds (with atomic displacement along the circumferential direction) in the tube; and (8) the medium peak at 1650 cm^{-1} is as a result of the CC stretching and bending deformation of CCC bonds in the benzene, accompanied by rocking (in-plane motion) of the Hs on the benzene ring.

(c) Calculated new Raman features in the spectrum of the (7,0)-SWCNT-CO_2H: (1) a relatively strong at 1123 cm^{-1} result from the symmetric stretching vibration of the CCC bonds (where–CO_2H unit is covalently attached on the sidewall of the tube), including bending deformation of the CCC bonds in the tube, including inplane rocking of Hs on the benzene ring; (2) a medium intense peak 1146 cm^{-1} is due to asymmetric stretching of C—C=O and rocking of OH bond in the —CO_2H group, including structural deformation of the tube; (3) a strong at 1376 cm^{-1} is as a result of structural deformation of the tube; (4) there are two peaks:) one with relatively weak at 1385 cm^{-1} is due to the asymmetric stretching vibration of the CCO(H) and bending deformation of the CCC bonds in the tube; other strong one at 1391 cm^{-1} is caused by asymmetric stretching vibration of the CCC bonds in the tube, no contribution from

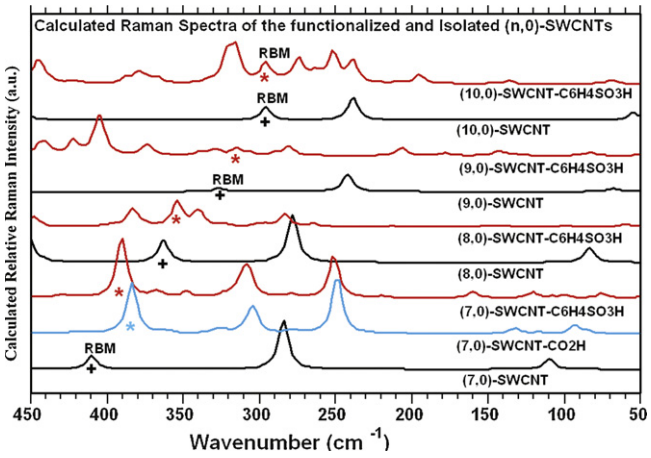

Fig. 3. Calculated RBMs of frequencies in Raman spectra of the (*n*,0)-SWCNT-ph-SO_3H, (7,0)-SWCNT-CO_2H, and isolated (*n*,0)-SWCNTs: *n* = 7–10. Where the signs * and + indicate the RBMs for the functionalized and isolated SWCNTs, respectively.

the functional group (—CO_2H); (5) a medium peak at 1472 cm^{-1} is caused by structural deformation of the tube; (6) medium peak at 1549/1557 cm^{-1} is due to the stretching vibrations CC bonds (with atomic displacement along the circumferential direction) in the tube; and (7) the weak peak at 1806 cm^{-1} is as a result of the C=O stretching and bending deformation of COH bond in the carboxylic acid.

(d) Calculated CH and OH bond stretching vibrations in the Raman spectrum of the functionalized and isolated (7,0)-SWCNT: while the stretching of CH bonds on the open-end of the tube are predicted in the range of 3172–3200 cm^{-1}, the CH stretching vibration of the benzene ring in the benzenesulfonic acid are in the range of 3200–3240 cm^{-1}. The OH bond stretching vibration is shown at 3703 cm^{-1} for the benzenesulfonic acid and at 3678 cm^{-1} for the carboxylic acid.

The key conclusions of these calculations on the (0,*n*)-SWCNT-ph-SO_3H (*n* = 6–11) and (7,0)-SWCNT-CO_2H, with reference to the spectrum of their corresponding isolated (0,*n*)-SWCNT, are summarized as: (a) As seen in Fig. 3, the calculated Raman spectra of the (0,*n*)-SWCNT-ph-SO_3H (*n* = 6–11) and (0,*n*)-SWCNT-CO_2H indicated that the calculated redshift in the peak positions of the RBMs (relative to corresponding one in the spectrum of their corresponding isolated (0,*n*)-SWCNT)) increases with decreasing tube diameter, which is consistent with experimental observation [51]. This red shifting of the RBMs for both spectra is a result of the structural deformation of the SWCNTs caused by the surface chemical functionalization; (b) the calculated Raman spectra of the f-(0,*n*)-SWCNT not only exhibited many new peaks in the disorder (D) mode range of ~1300 to ~1400 cm^{-1}, but also the D to G band intensity ratio (I_D/I_G) ratio which is the intensity of the disorder mode as observed experimentally [51,52]. Experimental studies have showed that the increase in the I_D/I_G ratio indicates an increase in the number of defects on the sidewall of the nanotube [52,53]. (c) In the range of the tangential (G) mode (1500–1600 cm^{-1}), as a result of the chemical functionalization of the SWCNT with benzenesulfonic and carbocyclic acid (-ph-SO_3H and —CO_2H), not only the G-band at 1574 cm^{-1} in the Raman spectrum of the (0,7)-SWCNT is blue shifted to ~1590 and 1595 cm^{-1} in the Raman spectra of the (7,0)-SWCNT-ph-SO_3H and (7,0)-SWCNT-CO_2H, respectively, but also G-band of frequency in the spectrum of the (7,0)-SWCNT-CO_2H is also blue shifted (5 cm^{-1}) relative to that in the (7,0)-SWCNT-ph-SO_3H. As discussed above, other new Raman Features in this G-mode region appeared in the range of 1500–1600 cm^{-1} in the spectrum of the f-(0,*n*)-SWCNTs; (d) above the G-mode, the spectrum of the f-(7,0)-SWCNT exhibited a new Raman feature which belongs to the functional groups only: at 1650 cm^{-1} in the spectrum of the (7,0)-SWCNT-ph-SO_3H and at 1806 cm^{-1} in the spectrum of the (7,0)-SWCNT-CO_2H; (e) CH and OH bond stretching vibrations for the tube and different functional groups are well separated from each other as discussed above. These peaks also may be a signature for the functionalized nanotube.

As it is well known, the calculations using DFT techniques overestimates the value of the vibrational frequencies when comparing with their experimentally observed values. Based on our experiences with organic molecules and transition metal clusters, and other published studies indicated that theoretical values generally perfectly match with the experimental ones when using a scaling factor in the range of 0.96–1.00 [26,27,45–50]. It is worth nothing that the relative intensity of the peaks in the resonance Raman spectra significantly change. Because of the technical difficulty and calculation time, it is very difficult to calculate resonance Raman spectra (RRS).

Furthermore, in the low frequency region below 600 cm^{-1}, there are many vibrational Raman mode (with relatively very weak or vanish intense), which result from out-of-plane motion, or twisting of the phenyl group. These types of Raman bands of the functionalizated the CNTs may significantly enhanced in the resonance Raman spectrum (RRS) since there is a significant π–π^* or dipole-dipole interaction between the functional groups. This may play a crucial role and might be used as signature for the alignment of the CNTs in two dimensional networks, but also, the presence of additional bands may lead to the erroneous conclusion on the position of the RBM and/or existence of more than one type of SWNT in the sample. For instance, the Raman band(s) resulting from out-of-plane motions are dramatically enhanced when dye molecule aggregate, and are referred to as J- or H- type aggregates. This is due to the π–π^* interactions between the molecules such as aromatic chromophores, which are expected to play dominant roles in holding the aggregate together. Due to out-of-plane motions of the aromatic groups, even in-plane motions, these vibrational motions of the aromatic groups are expected to be amplified through induced electronic distribution changes in adjacent aromatic chromophores leading to increased polarizability of the aggregate structure and not only enhanced Raman scattering, but also, leading to new Raman in the range of 100–500 cm^{-1}. For more detail, see the text in references 47,48,49,50).

3.3. *IR spectra of functionalized zigzag-SWCNTs*

Bt Asari @ Mansor et al. [53] have studied surface functionalization of multi-walled carbon nanotubes (MWCNTs) have been investigated using a gas phase treatment in a Universal Temperature Program (UTP) reactor by flowing SO_3 gas onto the CNTs while being heated at different temperatures. They characterized the functionalized nanotubes using Fourier transform infrared spectroscopy (FT-IR) and Raman spectroscopy. Their measured IR spectra exhibited broad IR peaks. During the assignment our calculated IR spectra of the functionalized and isolated nanotube, we will use these information for comparison.

The calculated IR spectra of the f-(*n*,0)-SWCNT ((*n*,0)-SWCNT-ph-SO_3H and (*n*,0)-SWCNT-CO_2H, *n* = 6–11) and the spectra of their corresponding isolated (*n*,0)-SWCNTs are given in Fig. S2 in supplementary information (SI). In order to determine the dependence of the IR spectrum on the sidewall functionalization of a desired (*n*,0)-SWCNT with different types of functional groups, at same level of the theory, we also calculated the IR spectrum of the isolated (7,0)-SWCNT with carboxylic acid ((7,0)-SWCNT-CO_2H) for comparison with that of the (7,0)-SWCNT-ph-SO_3H system. Because of the similarity of the IR spectra of the f-(*n*,0)-SWCNTs, here we discuss only the IR spectra of the (7,0)-SWCNT-ph-SO_3H and

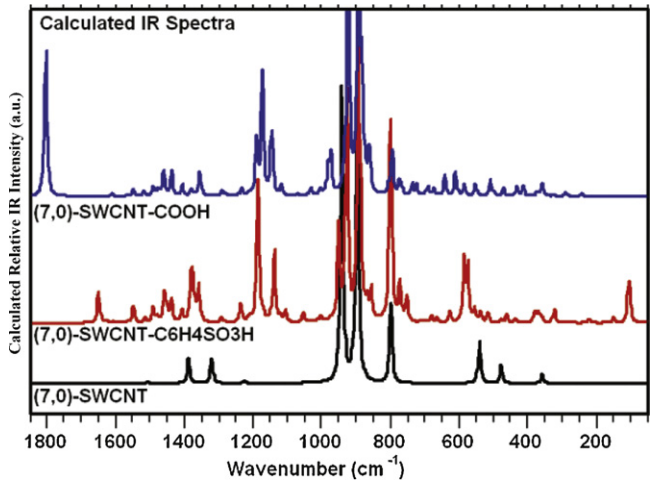

Fig. 4. Calculated IR spectra of the (7,0)-SWCNT-ph-SO_3H, (7,0)-SWCNT-CO_2H, and isolated (7,0)-SWCNT.

(7,0)-SWCNT-CO_2H. The results of the calculated IR spectra of the f-(7,0)-SWCNT and isolated (7,0)-SWCNT are summarized below.

(a) The predicted common peaks in the IR spectra of the functionalized and isolated (7,0)-SWCNT: the calculated IR spectra of the (7,0)-SWCNT produced eight peaks: (1) One of them at 358 (weak) cm^{-1} (due to motion of the carbon atoms in radial directions that leads to the shape of the tube like a pinecone form), which is blue shifted to 380 (weak) and 375 (weak) cm^{-1} in the spectra of (7,0)-SWCNT-ph-SO_3H and (7,0)-SWCNT-CO_2H, respectively; (2) The calculated peaks at 477 (weak), as result of the out-of-surface bending deformation of the tube, is blue shifted to 515 (weak) and 510 (weak) cm^{-1} in the spectra of (7,0)-SWCNT-ph-SO_3H and (7,0)-SWCNT-CO_2H, respectively; (3) A medium intense peak at 541 cm^{-1} (caused by the out-of-surface bending deformation of the tube) is not only shifted to ~552 cm^{-1} in the spectra of both f-(7,0)-SWCNT, but also, its intensity dramatically decreased in both spectra; (4) the most strongest peak at 799 cm^{-1} are caused by twisting of the CCC bonds in the tube such as the out-of-surface bending deformation, which is found to appear almost at the same position in both spectra; however, the intensity of the corresponding peak (at 801 cm^{-1}) in the spectrum of the (7,0)-ph-SO_3H is relatively stronger than its intensity in the spectra of the (7,0)-SWCNT-CO_2H and (7,0)-SWCNT because there is a significant contribution comes from the asymmetric stretching of the CSO(H) bonds, including expansion of the benzene ring along radial direction of the tube, in addition to the twisting of the CCC bonds in the tube. In the case of (7,0)-SWCNT-CO_2H, there is no significant contribution from the carboxylic acid to this peak (predicted at 797 cm^{-1}). This calculated peak is consistent with the observed broad peak centered 770 cm^{-1} in the FT-IR spectra of the functionalized nanotube by Bt Asari @ Mansor et al. [53], which was attributed to CS stretching mode by the author. (5) As seen in Fig. 4, the predicted two stronger peaks at 896 and 941 cm^{-1} in the IR spectra of the (*n*,0)-SWCNTs is as a result of the out-of-surface bending deformation of the tube, including significant contribution from the wagging of the Hs on the open-end of the SWCNTs. These peaks are predicated at 894 and 926 cm^{-1} in the IR spectra of both f-(*n*,0)-SWCNTs; (6) A relatively very weak peak at 1224 cm^{-1} (due to the structural deformation of the tube) is blue shifted to 1236 and 1233 cm^{-1} in spectra of the (7,0)-SWCNT-CO_2H and (7,0)-SWCNT, respectively, and no change in its relative intensity; (7) the peak at 1320 cm^{-1} (results from bending deformation of the tube) is red shifted to 1292 cm^{-1} and its intensity dramatically decreased in the IR spectra of both (7,0)-SWCNT-CO_2H and (7,0)-SWCNT; (8) The medium intense peak at 1387 cm^{-1} (caused by stretching of CC bond in the tube) is not only blue shifted to 1407 cm^{-1} in both spectra, but also, its intensity almost vanishes.

(9) A very weak peak at 1507 cm^{-1} (as a result of CC stretching in tube) is red shifted to 1492 cm^{-1} in both spectra and no change its intensity.

(b) Calculated new IR features in the spectrum of the (7,0)-SWCNT-ph-SO_3H: (1) the peak at 105 cm^{-1} is mainly due to the rocking of the OH bond, including relatively weak twisting of O═S═O bond and out-of-plane wagging of the benzene ring; (2) the medium peaks at 573 and 585 cm^{-1} are owing to the out-of-plane bending deformation of the benzene ring (boating) and wagging of Hs on the benzene ring, including bending deformation of the SO_3H group like an open and close umbrella shape. This vibrational mode corresponds to the observed IR peak at around 580 cm^{-1} even though the author did not mention, in their assignment of the measured IR spectrum; (3) relatively weak features at 753 cm^{-1} is as a result of the symmetric stretching vibration of the CSO(H) bonds, including bending deformation in the benzene ring; (4) The author [53] suggested that the observed peak at 860 cm^{-1} can be due to SOC stretching group. However, the calculated IR spectra did not exhibit any IR peaks involve the vibrational motions of the SO_3H in the range of 805–1076 cm^{-1}. Therefore, the calculated peaks at 857 and 867 cm^{-1} might be responsible for this observed peak at 860 cm^{-1}, which is caused by wagging of Hs on benzene ring, including out of surface motion of the C atom in tube, which is bound to functional group. (5) a relatively strong peak at 950 cm^{-1} is due to out-of-surface vibrational motion of the C atom in the tube, which is bound to the benzenesulfonic acid (-ph-SO_3H), including breathing of the benzene ring; (6) a medium peak at 1138 cm^{-1} is mainly due to asymmetric stretching of the —C—S═O bond and rocking of the OH in SO_3H group, accompanied by rocking of CHs on the benzene ring; (7) a strong peak at 1186 cm^{-1} is originating from symmetric stretching of the O═S═O bond and rocking of the OH bond, including SC stretching. The latter two peaks (1138 and 1186 cm^{-1}) corresponds to a broad peak centered 1125 cm^{-1} in the observed IR spectra which was attributed to the SO_2 symmetric stretching mode by authors [53]; (8) two medium intense peaks at 1360 and 1373 cm^{-1} are as a result of asymmetric stretching of O═S═O bond and OH rocking, including asymmetric stretching of CCC in the benzene ring; (9) two weak peaks at 1437 and 1458 cm^{-1} are caused by symmetric stretching of CCC in the tube. (10) The authors [53] measured a considerably broadened peak centered 1540 cm^{-1} in the observed spectrum and they suggested that this broadened peak was due to the C═C stretching mode which originates from the backbone of carbon nanotubes. This peak corresponds to our calculated peak at 1546 cm^{-1}, which is caused by symmetric stretching of CCC bonds in the benzene ring and rocking of Hs on the ring; (11) a medium peak at 1650 cm^{-1} is as a result of the CC bonding stretching and bending deformation of CCC bonds in the benzene ring.

(c) Calculated new IR features in the spectrum of the (7,0)-SWCNT-CO_2H) are: (1) the new peaks below 600 cm^{-1} result from the rocking of CO_2H group and structural deformation of the tube; a weak peak at 612 cm^{-1} is due to the wagging of OH; (2) a weak peak at 644 cm^{-1} is as a result of the bending deformation of the O═C—O and wagging of OH; (3) The observed peak at 1011 cm^{-1} was assigned to CO stretching by author, which corresponds to two medium intense peaks at 976 and 984 cm^{-1} are caused by symmetric stretching vibration of CCO(H) bonds; (4) two medium intense peaks at 1148 and 1192 cm^{-1}, and a strong peak at 1175 cm^{-1} are originating from asymmetric stretching of —C—C—O(H) and rocking of OH, including relatively weak structural deformation of the tube; (5) a weak peak at 1358 cm^{-1} results from bending deformation of COH in the —CO_2H functional group; (6) two weak peaks at 1438 and 1463 cm^{-1} are due to structural deformation of the tube; (7) The most strong peak at 1806 cm^{-1} is as a result of C═O stretching

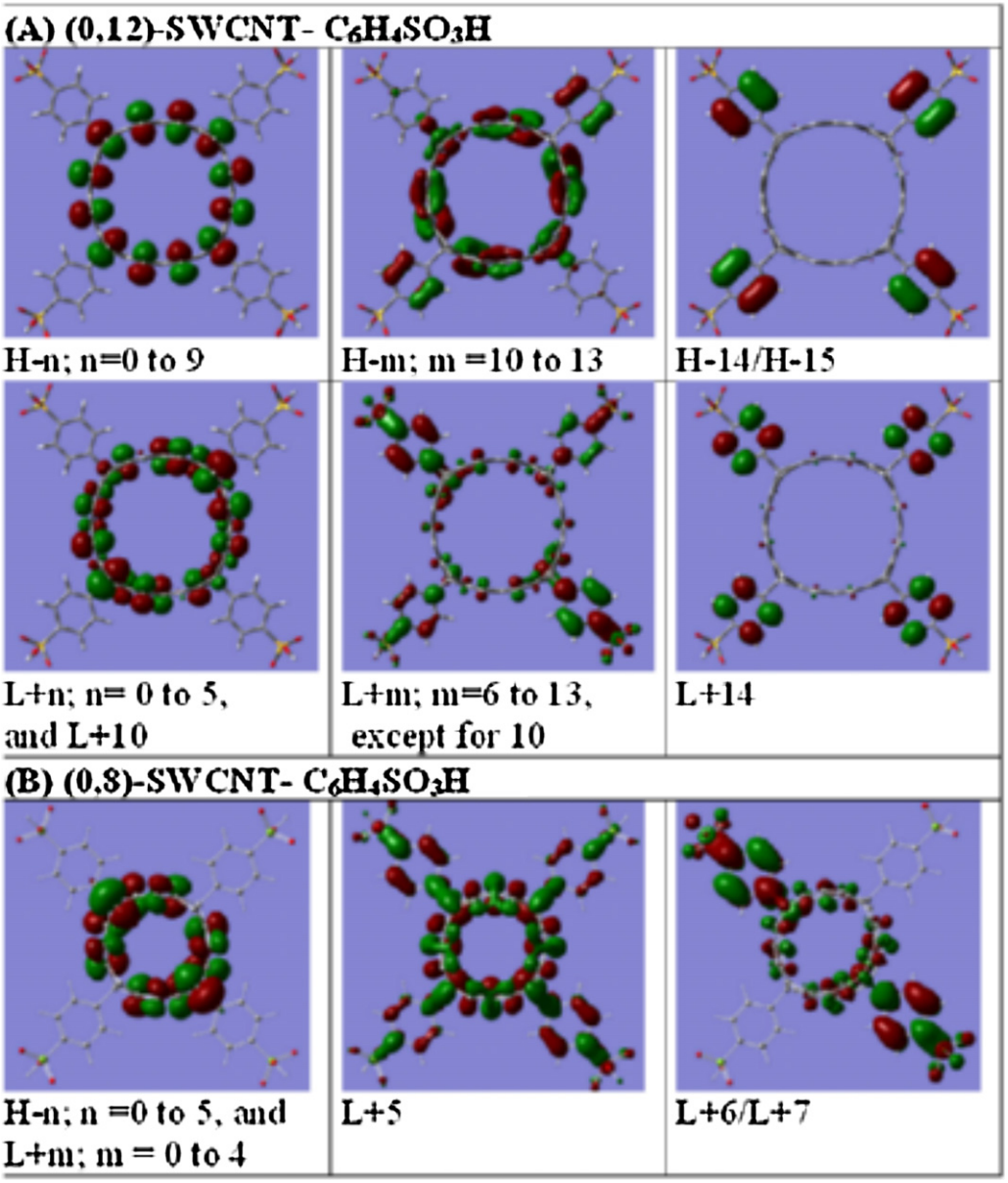

Fig. 5. Calculated electron densities in the HOMO and LUMO states for the covalent sidewall functionalization of the (*n*,0)-SWCNT (*n* = 8,9,12) with benzenesulfonic acid (—$C_6H_4SO_3H$). The functionalized-SWCNTs constructed as four functional group covalently attached on the (*n*,0)-SWCNTs with length equivalent to two unit.

and bending deformation of COH, which is experimentally observed at 1782 cm^{-1} in the FTIR spectra of MWCNT after electron-beam irradiation by Lee et al. [54]. However, Bt Asari @ Mansor et al. [53] measured a strong peak at 1702 cm^{-1} in the FT-IR spectrum and they were attributed this peak to the C=O stretching mode of the —COOH groups.

Furthermore, the calculated IR peaks in the range of 3000–4000 cm^{-1}, the CH stretching mode in the range of 3214–3240 cm^{-1}; OH stretching mode at 3703 cm^{-1} (in the SO3H group) and at 3678 cm^{-1} (in the CO2H group). These calculated IR peaks are in good agreement with measured IR features in the range of 3175–3785 cm^{-1}. The calculated CH stretching predicted in the range of 3172–3203 cm^{-1} for the isolated (7,0)-SWCNTs.

The key conclusion on the IR spectra of the f-(7,0)-SWCNT, with reference to the isolated (7,0)-SWCNT, is that they exhibits new IR features along the spectrum and the intensities of some IR peaks are enhanced or decrease. Again, it should be point out that the calculated peak positions may be larger than their experimental values; therefore, they are usually fitted by using a scale factor range from 0.96 to 1.00. As a result, the calculations clearly indicated that the IR spectroscopy as well as the Raman spectroscopy can provide very useful information about functionalized and isolated nanotubes for their characterizations.

3.4. Vertical electronic transitions of functionalized zigzag-SWCNTs

We calculated the vertical electronic transitions for the sidewall functionalization of (*n*,0)-SWCNTs with the benzenesulfonic acid (-ph-SO_3H). The functionalized-SWCNTs constructed as two functional groups (-ph-SO_3H) covalently attached to the (9,0)- and (7,0)-SWCNT, and four functional groups bound to the (12,0)- and (8,0)-SWCNTs with length equivalent to two unit as seen in Fig. 5. While Table 1 provides calculated electronic transitions of the functionalized and the isolated SWCNTs, the calculated electron density in the HOMOs and LUMOs states which are involved in the vertical

Table 1
Calculated vertical electronic transition energies (T_e; in eV) of the sidewall functionalization of the (0,*n*)-SWCNTs with benzenesulfonic acid ((0,*n*)-SWCNTs-ph-SO_3H) with that for the isolated (0,*n*)-SWCNTs for comparison with their oscillator strengths (*f*). Where the signs: # and * indicates four and two functional groups covalently bound to the (0,*n*)-SWCNTs, respectively.

	(12,0)-SWCNT		f-(12,0)-SWCNT#		(8,0)-SWCNT		f-(8,0)-SWCNT#		(9,0)-SWCNT		f-(9,0)-SWCNT*		(7,0)-SWCNT		f-(7,0)-SWCNT*	
	T_e (eV)	*f*	T_e (eV)	*f*	T_e (eV)	*f*	T_e (eV)	*f*	T_e (eV)	*f*	T_e (eV)	*f*	T_e (eV)	*f*	T_e (eV)	*f*
1	0.54	0.0076	0.12	0.0001	0.77	0.0164	0.09	0.0001	0.56		0.27		0.91		0.39	
2	0.82		0.15	0.0001	1.46	0.0006	0.11		0.80		0.30	0.0144	1.25		0.79	0.0573
3	0.82		0.16	0.0001	1.46	0.0006	0.14		0.80		0.57		1.25		1.07	0.0067
4	1.27		0.42		2.44		0.31	0.0003	0.93	0.0391	0.83	0.0087	1.45	0.0647	1.11	
5	1.51		0.55	0.0111	2.51	0.3588	0.36	0.0059	2.32		1.34		2.52			
6	1.51		0.55	0.0113	2.51	0.3588	0.55	0.0013	2.32		1.46	0.0307	2.53			
7	1.71	0.1082	0.65	0.0356	2.53		0.62		2.50		1.47	0.1432	2.93			
8	1.87	0.6641	0.65	0.0355	2.77		0.79		2.50		1.57		2.93			
9	1.87	0.6641	0.74	0.0101	2.77		0.93	0.0462	2.64		1.64		3.02			
10	2.31		1.10	0.0054	2.78		1.86	0.0049	2.64		1.84		3.02			
11	2.31		1.10	0.0053	2.78		1.91		2.72		1.88		3.08			
12	2.56		1.37	0.0072	2.98	0.1295	1.96	0.0022	2.72		1.88	0.0268	3.08			
13	2.76		1.37	0.0071			2.00				2.10					
14	2.76		1.49				2.09	0.0002			2.11	0.0020				
15	2.81		1.50				2.12	0.0010			2.19					
16	2.82		1.52	0.0060			2.18				2.24	0.0272				
17	2.82		1.55				2.21	0.0031								
18	2.94		1.63	0.0137			2.24	0.0043								
19	2.94		1.63	0.0137			2.27	0.0236								
20	2.99		1.70	0.0014			2.29	0.0157								
21	2.99		1.70	0.0014			2.30									
22	3.03		1.78				2.36	0.0018								
23	3.03		1.89				2.38									
24	3.18	0.0301	2.04	0.2005			2.41	0.0015								
25			2.04													
26			2.05	0.2018												
27			2.18	0.1953												
28			2.18	0.1954												
29			2.21	0.0017												
30			2.23													
31			2.41	0.0015												
32			2.41	0.0016												
33			2.44													
34			2.51													
35			2.52	0.0002												
36			2.55													

electronic transitions are provided in Fig. 5A and B. All calculated electron densities and the contributions of each HOMOs → LUMOs transitions (with the configurationally interaction coefficients to each electronic states are given in supplementary information (SI). The results of the calculations clearly indicated that both, the dipole allowed and forbidden electronic transitions, are lowered as much as 0.8 eV with comparison to the transition energies of their corresponding isolated (*n*,0)-SWCNT.

The calculated vertical electronic transitions up to 2.53 eV exhibited many dipole allowed and forbidden electronic transitions. When we examine the electronic transitions and calculated electron densities in HOMOs and LUMOs together for the (12,0)-SWCNT-ph-SO_3H, we see that while the calculated electronic transitions below 2.0 eV did not indicate any charge transfer state, which result from HOMOs to LUMOs of the SWCNT only. Nevertheless, above the 2.04 eV, the calculation indicates the existence of the charge transfer states from the HOMOs of (12,0)-SWCNT to the LUMOs of the benzenesulfonic acid ($-C_6H_4SO_3H$). For instance, the dipole allowed electronic transitions: $S_0 \rightarrow S_{29}$ (T_e = 2.208 eV) results from the HOMO of the SWCNT to the LUMO + 8 of the benzenesulfonic acid only. The transitions $S_0 \rightarrow S_{24}/S_{25}$ (T_e = 2.040/2.041 eV) and $S_0 \rightarrow S_{27}/S_{28}$ (T_e = 2.179/2.180 eV) dipole-allowed electronic transitions are due to the transitions to the LUMOs of both the benzenesulfonic acid and the SWCNT from the HOMOs of the SWCNT. As seen in Table 1 and in the SI, there are many dipole allowed electronic transitions from the HOMO of the SWCNT to the LUMOs of both SWCNT and the benzenesulfonic acid. The results of the calculated vertical electronic transitions of the functionalized nanotube ((12,0)-SWCNT-ph-SO_3H) indicated that there is a charge transfer mechanism from the nanotube to the molecule above 2.0 eV. Furthermore, the small distances between the electronic transitions suggest that there would be an internal conversion (IC) via vibrational coupling. These spectroscopic properties, the charge transfer process and the IC, can be experimentally observable by quenching in florescence and enhanced or new Raman features in the measured resonance Raman spectrum as well as these in the IR spectrum [51].

For the (8,0)-SWCN-ph-SO_3H, we calculated the vertical electronic transitions up to 2.41 eV. When we examine the calculated energy levels and the electron densities of the HOMOs and LUMOs (Fig. 5B) together, we see that the calculated electronic transitions up to 1.91 eV did not indicate any charge transfer process, however, the calculated electronic transitions above the 1.91 eV showed many dipole allowed and forbidden electronic transitions from the HOMOs of the isolated SWCNT to LUMOs of the benzenesulfonic acid and SWCNT coming such as: $S_0 \rightarrow S_{12}$ (T_e = 1.96 eV) due to H-3 → L, H-1 → L + 3, and H → L + 5 (where charge transfer (CT) takes place); $S_0 \rightarrow S_{14}$ (T_e = 2.09 eV) due to H-3 → L, H-1 → L + 3, and H → L + 5 (where CT takes place); $S_0 \rightarrow S_{18}$ (T_e = 1.24 eV) due to H-1 → L + 5 and H → L + 7 (where charge transfer (CT) takes place) including H-4 → L; $S_0 \rightarrow S_{19}$ (T_e = 2.27 eV) due to H-6 → L, H-4 → L + 1, H-3 → L, H-1 → L + 3, and including H → L + 5 (where charge transfer (CT) takes place); $S_0 \rightarrow S_{22}$ (T_e = 2.36 eV) due to H-6 → L, H-5 → L + 2, H-4 → L + 1, H-2 → L + 3, and H → L + 8 (where charge transfer (CT) takes place); $S_0 \rightarrow S_{24}$ (T_e = 2.41 eV) due to H → L + 5/L + 8 (where charge transfer (CT) takes place) including H-5 → L + 2.

The electronic structure of the functionalized-single-walled carbon nanotubes, f-(9,0)-SWCNTs, build with two functional groups covalently bound to the (9,0)-SWCNTs with length equivalent to two unit cell, have been investigated. The results of the calculated electronic transition of the (9,0)-SWCNT functionalizes with benzenesulfonic acid are lowered in electronic energy levels with relation to the isolated (9,0)-SWCNT and also indicated many dipole-allowed and forbidden electronic transitions as seen in Table 1. All of the calculated electronic transitions and all electron densities in the HOMOs and LUMOs states with the configurationally interaction coefficients are given in Table S3 in supplementary information. Similar calculations performed to the (12,0)-SWCNT-ph-SO_3H and (8,0)-SWCNT-ph-SO_3H, showed charge transfer from the nanotube to molecule: $S_0 \rightarrow S_{14}$ (T_e = 2.11 eV, dipole-allowed) due to H → L + 5 (CT takes place) and minor contribution from H-1 → L + 3 transition. Furthermore, there are a few dipole-forbidden electronic transitions where the CT takes place as well as many electronic transitions which result from HOMOs to LUMOs of the (9,0)-SWCNT.

It is worth noting that when the absorption of a photon promotes the molecule from ground state (singlet state, S_0) to the first excited state singlet state (S1) or upper excites singlet state (S_k, $k > 1$). The excited molecule eases to the lowest vibrational level of the first excited state through internal conversion (IC), also known as vibrational relaxation, and the process takes about a picosecond. An excited molecule exists in the lowest excited state (S_1) for a period of about nanoseconds, and relaxes back to the ground state by one of the three mechanisms: For instance, when the SWCNT is excited by absorption of a photon, the species [SWCNT]* is left in a charge transfer excited state – an electron is transferred from the SWCNT to the antibonding orbitals of the functional group. The excited state may undergo a variety of processes, such as: (1) SWCNT + hν → [SWCNT]* (absorption); (2) [SWCNT]* → SWCNT (Fluorescence, IC or non-radiative decay, and ISC); and (3) [SWCNT]* + functional group → [SWCNT]$^+$ + [functional group]$^{-1}$ (quenching). The first step is the excitation process; the second represents all processes other than quenching which lead to the excited molecule returning to the ground state. The final step represents the loss of energy by quenching, which can occur through a variety of mechanisms, depending upon the identity of the quenching species.

4. Conclusion and remarks

Raman spectroscopy is one of the most extensively employed methods for exploring the modification of the electronic and vibrational properties of carbon nanotubes caused by various chemical functionalization strategies. The calculated Raman spectra of the (7,0)-SWCNT-ph-SO_3H produced new features with respect to corresponding one in the spectrum of the isolated-SWCNT. Some of these are predicted at: 1119, 1139, 1373, 1502, 1547 and 1557, and 1650 cm^{-1} (see in the text for their mode assignments). The calculations also showed a significant enhancement in the intensity of the Raman peaks, such as the peaks at 1302 and 1389 cm^{-1} in the range of the disorder (D) mode, in the range of ~1300 to ~1400 cm^{-1}. The Calculations also indicated that the predicted red shifting of the RBMs for f-(0,*n*)-SWCNTs (*n* = 6–10) is a result of the structural deformation of the SWCNTs caused by the surface chemical functionalization. The calculated Raman spectra of the (7,0)-SWCNT-ph-CO_2H also exhibited similar new features such as at 1123, 146, 1376, 1391, 1472,1549, and 1557, and 1806 cm^{-1} (see in the text for their assignments).

The calculations indicated that the calculated IR spectra of the (0,7)-SWCNT-ph-SO_3H and (0,7)-SWCNT-CO_2H are in good agreement with the most of the observed peaks in the measured IR spectra [53] as discussed above. The calculated f-(0,7)-SWCNT also exhibited new IR peaks in relation to corresponding one in the spectrum of the isolated-(0,7)-SWCNT. Some of these peaks are predicted at 585, 753, 1138, 1186, 1360 and 1373, 1546, and 1650 cm^{-1}(see in text for their full assignments). For the (0,7)-SWCNT-CO_2H, some of the new IR features are predicted at 644, 976, 984, 1148,1175 cm^{-1}, 1192, 1358, and 1806 cm^{-1}. These calculated characteristic Raman and IR features may provide a

signature of covalent functionalization of the carbon nanotubes (f-CNT). The calculations also CH stretching in the benzene ring (3172–3200 cm^{-1}), $-CO_2H$ are well separated (3678 cm^{-1}), and $-SO_3H$ (3703 cm^{-1}). These theoretical values might be somewhat higher than their experimental values and can be fitted by using a scaling factor in the range of 0.96–1.

The calculated vertical electronic transitions up to 2.5 eV exhibited many dipole-allowed and forbidden electronic transitions for the f-SWCNTs. While the calculated electronic transitions below about 2.0 eV did not predict any charge transfer state, above 2.0 eV, the calculation leisure indicate the existence of the charge transfer states to the LUMOs of the benzenesulfonic acid ($-C_6H_4SO_3H$) coming from the HOMOs of the isolated (12,0)-SWCNT. The small distance between the electronic transitions suggested that there would be an internal conversion (IC) process happening via vibrational coupling, which can modify the optical spectra and dynamics of the functionalized nanotube. It is worth mentioning that the intersystem crossing (ISC) processes as well as the photochemical and other photophysical processes are under investigation for various types of functionalized SWCNTs.

Appendix A. Supplementary data

Supplementary data associated with this article can be found, in the online version, at http://dx.doi.org/10.1016/j.vibspec.2012.12.003.

References

[1] S. Iijima, Nature 354 (1991) 56.
[2] D. Nepal, J.I. Sohn, W.K. Aicher, S. Lee, K.E. Geckeler, Biomacromolecules 6 (6) (2005) 2919.
[3] S.S. Karajanagi, H. Yang, P. Asuri, E. Sellitto, J.S. Dordick, R.S. Kane, Langmuir 22 (2006) 1392.
[4] H. Finkelstein, P.M. Asbeck, S. Esener, 3rd IEEE Conference on Nanotechnology (IEEE-NANO), vol. 1, 2003, p. 441.
[5] C. Zhou, J. Kong, E. Yenilmez, H. Dai, Science 290 (2000) 1552.
[6] J.A. Misewich, R. Martel, P. Avouris, J.C. Tsang, S. Heinze, J. Tersoff, Science 300 (2003) 783.
[7] A. Nitzan, R.A. Ratner, Science 300 (2003) 1384.
[8] D.S. Wen, Y.L. Ding, Int. J. Heat Mass Transfer 47 (2004) 5181.
[9] Y. Ding, H. Chen, L. Wang, C.-Y. Yang, Y.g. He, W. Yang, W.P. Lee, L. Zhang, R. Huo, KONA 25 (2007) 23.
[10] C.S. Jones, X. Lu, M. Renn, M. Stroder, W.S. Shih, Microelectron. Eng. 87 (2010) 434.
[11] S.M. Jung, H.Y. Jung, J.S. Suh, Sens. Actuator B: Chem. 139 (2009) 425.
[12] T. Rueckes, K. Kim, E. Joselevich, G.Y. Tseng, C.L. Cheung, C.M. Lieber, Science 289 (2000) 94.
[13] M.J. O'Connell, S.M. Bachilo, C.B. Huffman, V.C. Moore, M.S. Strano, E.H. Haroz, K.L. Rialon, P.J. Boul, W.H. Noon, C. Kittrell, J. Ma, R.H. Hauge, R.B. Weisman, R.E. Smalley, Science 297 (2002) 593.
[14] S.M. Bachilo, M.S. Strano, C. Kittrell, R.H. Hauge, R.E. Smalley, R.B. Weisman, Science 298 (2002) 2361.
[15] A. Hartschuh, H.N. Pedrosa, L. Novotny, T.D. Krauss, Science 301 (2003) 1354.
[16] J. Maultzsch, R. Pomraenke, S. Reich, E. Chang, D. Prezzi, A. Ruini, E. Molinari, M.S. Strano, C. Thomsen1, C. Lienau, Phys. Status Solidi B 243 (13) (2006) 3204.
[17] E. Chang, G. Bussi, A. Ruini, E. Molinari, Phys. Rev. Lett. 92 (2004) 196401.
[18] C.D. Spataru, S. Ismail-Beigi, L.X. Benedict, S.G. Louie, Phys. Rev. Lett. 92 (2004) 077402.
[19] V. Perebeinos, J. Tersoff, P. Avouris, Phys. Rev. Lett. 92 (2004) 257402.
[20] M. Zheng, A. Jagota, E.D. Semke, B.A. Diner, R.S. McLean, S.R. Lustig, R.E. Richardson, N.G. Tassi, Nat. Mater. 2 (2003) 338.
[21] W. -Il Park, H.S. Kim, S.M. Kwon, Y.H. Hong, H.J. Jin, Carbohyd. Polym. 77 (2009) 457.
[22] L. Meng, C. Fu, Q. Lu, Prog. Nat. Sci. 19 (7) (2009) 801.
[23] C.T. Hsieh, Y.T. Lin, Microporous Mesoporous Mater. 93 (2006) 232.
[24] J.J. Davis, K.S. Coleman, B.R. Azamian, C.B. Bagshaw, M.L.H. Green, Chem. Eur. J. 9 (16) (2003) 3732.
[25] V.Z. Poenitzsch, D.C. Winters, H. Xie, G.R. Dieckmann, A.B. Dalton, I.H. Musselman, J. Am. Chem. Soc. 129 (47) (2007) 14724.
[26] M. Aydin, D.L. Akins, Vib. Spectrosc. 53 (2010) 163.
[27] M. Aydin, D.L. Akins, in: J.M. Marulanda (Ed.), Geometric and Spectroscopic Properties of Carbon Nanotubes and Boron Nitride Nanotubes, Electronic Properties of Carbon Nanotubes, InTech, 2011, ISBN: 978-953-307-499-3, Available from: http://www.intechopen.com/books/electronic-properties-of-carbon-nanotubes/geometric-and-spectroscopic-properties-of-carbon-nanotubes-and-boron-nitride-nanotubes
[28] P.J.F. Harris, Carbon nanotube science: Synthesis, Properties and Applications, Cambridge University Press, Cambridge, 2009.
[29] Ali Javey, Jing Kong (Eds.), Carbon Nanotube Electronics, Springer Science + Business Media, LLC, 233 Spring Street, New York, NY 10013, USA, 2009.
[30] L. Alvarez, Y. Almadori, R. Arenal, R. Babaa, T. Michel, R.L. Parc, J.-L. Bantignies, B. Jousselme, S. Palacin, P. Hermet, J.-L. Sauvajol, J. Phys. Chem. C 115 (24) (2011) 11898.
[31] P.C. Eklund, J.M. Holden, R.A. Jishi, Carbon 33 (7) (1995) 959.
[32] Z. Liu, X. Zhang, X. Yang, Y. Ma, Y. Huang, B. Wang, Y. Chen, J. Sheng, J. Nanosci. Nanotechnol. 10 (9) (2010) 5570.
[33] I. Robel, B.A. Bunker, P.V. Kamat, Adv. Mater. 17 (20) (2005) 2458.
[34] M. Olek, T. Busgen, M. Hilgendorff, M. Giersig, J. Phys. Chem. B 110 (26) (2006) 12901.
[35] K. Yanagi, K. Iakoubovskii, H. Matsui, H. Matsuzaki, H. Okamoto, Y. Miyata, Y. Maniwa, S. Kazaoui, N. Minami, H. Kataura, J. Am. Chem. Soc. 129 (16) (2007) 4992.
[36] Y. Saito, K. Yanagi, N. Hayazawa, H. Ishitobi, A. Ono, H. Kataura, S. Kawata, Jpn. J. Appl. Phys. 45 (12) (2006) 9286.
[37] C. Srinivasan, Curr. Sci. India 94 (2008) 300.
[38] T.A. Hilder, J.M. Hill, Curr. Appl. Phys. 8 (2008) 258.
[39] J. Clendenin, J. Kim, S. Tung, Proc of 2007 2nd IEEE conference on Nanotechnology, 2007, p. 1028.
[40] A. Bianco, K. Kostarelos, M. Prato, Curr. Opin. Biotech. 9 (2005) 674.
[41] N.W.S. Kam, M. O'Connell, J.A. Wisdom, H. Dai, Proc. Natl. Acad. Sci. 102 (2005) 11600.
[42] A.D. Becke, J. Chem. Phys. 98 (1993) 5648.
[43] M.J. Frisch, G.W. Trucks, H.B. Schlegel, G.E. Scuseria, M.A. Robb, J.R. Cheeseman, J.A. Montgomery Jr., T. Vreven, K.N. Kudin, J.C. Burant, J.M. Millam, S.S. Iyengar, J. Tomasi, V. Barone, B. Mennucci, M. Cossi, G. Scalmani, N. Rega, G.A. Petersson, H. Nakatsuji, M. Hada, M. Ehara, K. Toyota, R. Fukuda, J. Hasegawa, M. Ishida, T. Nakajima, Y. Honda, O. Kitao, H. Nakai, M. Klene, X. Li, J.E. Knox, H.P. Hratchian, J.B. Cross, V. Bakken, C. Adamo, J. Jaramillo, R. Gomperts, R.E. Stratmann, O. Yazyev, A.J. Austin, R. Cammi, C. Pomelli, J.W. Ochterski, P.Y. Ayala, K. Morokuma, G.A. Voth, P. Salvador, J.J. Dannenberg, V.G. Zakrzewski, S. Dapprich, A.D. Daniels, M.C. Strain, O. Farkas, D.K. Malick, A.D. Rabuck, K. Raghavachari, J.B. Foresman, J.V. Ortiz, Q. Cui, A.G. Baboul, S. Clifford, J. Cioslowski, B.B. Stefanov, G. Liu, A. Liashenko, P. Piskorz, I. Komaromi, R.L. Martin, D.J. Fox, T. Keith, M.A. Al-Laham, C.Y. Peng, A. Nanayakkara, M. Challacombe, P.M.W. Gill, B. Johnson, W. Chen, M.W. Wong, C. Gonzalez, J.A. Pople, Gaussian 03, Revision E.01, Gaussian, Inc., Wallingford CT, 2004.
[44] Gaussview 03, Gaussian, Inc., Wallingford, CT, 2003.
[45] M. Aydin, J.R. Lombardi, J. Phys. Chem. A 113 (2009) 2809.
[46] M. Aydin, "Photofragmentation Spectroscopy", VDM Verlag, 2009; ISBN: 3639152891.
[47] C. Guo, M. Aydin, H.R. Zhu, D.L. Akins, J. Phys. Chem. B 106 (2002) 5447.
[48] H. Guo, X. Zhang, M. Aydin, W. Xu, H.R. Zhu, D.L. Akins, J. Mol. Struct. 689 (2004) 153.
[49] M. Aydin, F. Jean-Mary, N. Stevens, D.L. Akins, J. Phys. Chem. B 108 (2004) 9695.
[50] W. Xu, M. Aydin, S. Zakia, D.L. Akins, J. Phys. Chem. B 108 (2004) 5588.
[51] E. Lewis, B.D. MacCraith, E. McGlynn, J.A. McLaughlin, G.D. O'Sullivan, A.G. Ryder, J.E. Walsh, Proc. SPIE 5826 (2005) 12.
[52] Y. Jeong, J. Kim, G.W. Lee, Colloid Polym. Sci. 288 (2010) 1.
[53] N. Bt Asari @ Mansor, J.-P. Tessonnier, A. Rinaldi, S. Reiche, M.G. Kutty, Sains Malays. 41 (5) (2012) 603.
[54] E.-J. Lee, J.-S. Yoon, M.-N. Kim, E.-S. Park, in: S. Yellampalli (Ed.), Preparation and Applicability of Vinyl Alcohol Group Containing Polymer/MWNT Nanocomposite Using a Simple Saponification Method, Carbon Nanotubes – Polymer Nanocomposites, InTech, 2011, ISBN: 978-953-307-498-6, Available from: http://www.intechopen.com/books/carbon-nanotubes-polymer-nanocomposites/preparation-and-applicability-of-vinyl-alcohol-group-containing-polymer-mwnt-nanocomposite-using-a-s.